

Effects of Ultrasonic Nanocrystal Surface Modification on the Residual Stress, Microstructure, and Corrosion Resistance of 304 Stainless Steel Welds



CHANG YE, ABHISHEK TELANG, AMRINDER GILL, XINGSHUO WEN,
SEETHA R. MANNAVA, DONG QIAN, and VIJAY K. VASUDEVAN

In this study, ultrasonic nanocrystal surface modification (UNSM) of 304 stainless steel welds was carried out. UNSM effectively eliminates the tensile stress generated during welding and imparts beneficial compressive residual stresses. In addition, UNSM can effectively refine the grains and increase hardness in the near-surface region. Corrosion tests in boiling $MgCl_2$ solution demonstrate that UNSM can significantly improve the corrosion resistance due to the compressive residual stresses and changes in the near-surface microstructure.

<https://doi.org/10.1007/s11661-017-4451-9>

© The Minerals, Metals & Materials Society and ASM International 2018

I. INTRODUCTION

AUSTENITIC stainless steels (SS) are widely used due to a good combination of mechanical properties, weldability, and corrosion resistance. However, AISI 304 SS welds are known to be susceptible to corrosion in chloride solution. Welding-induced tensile stresses in materials can be deleterious to the fatigue and corrosion resistance, as reported in the literature.^[1] Advanced mechanical surface treatment techniques have been used to modify the nature of the residual stresses. For example, shot peening (SP),^[2] laser shock peening (LSP),^[3–8] and low plasticity burnishing (LPB),^[9] have been reported to generate beneficial compressive residual stresses in the near-surface region of mechanical components. In addition, these advanced mechanical surface treatment techniques are reported to induce nanocrystallization on metal surfaces to improve mechanical properties.^[5,9]

Ultrasonic nanocrystal surface modification (UNSM)^[10–12] is an innovative surface processing technique that utilizes ultrasonic strikes to induce near-surface grain refinement, hardening, and compressive

residual stresses in metals. UNSM has been successfully used to process carbon steel,^[10,13] stainless steel,^[14] NiTi,^[15] Ti64,^[16] bulk metallic glass,^[17] and magnesium alloys^[18,19] for improved properties and performance. In a recent study, the effects of UNSM on the stress corrosion cracking behavior of low-carbon steel-welded joint were studied.^[20] 304 SS is the most widely used stainless steel in refineries, power plants, *etc.* where welds can be exposed to chloride corrosion. In another recent study, the effect of UNSM on the pitting corrosion of 304 SS was studied.^[21] It was observed that the grain refinement induced by UNSM resulted in greater Cr enrichment in the surface passive film and the breakdown and removal of inclusion particle, leading to higher pitting corrosion resistance. UNSM has also been reported to eliminate tensile residual stresses and impart compressive residual stresses in 3D-printed Ti64.^[16] Residual stresses play an important role in the properties of welds. It is thus worthy to study the effect of UNSM on the residual stress status of welds. Till now, the effects of UNSM on the microstructure, residual stresses, and properties of SS welds have not been studied. Considering that UNSM can eliminate surface tensile residual stresses and induce beneficial compressive residual stresses, it is thus important to investigate the effects of UNSM on the microstructure, residual stresses, and corrosion resistance of 304 SS welds.

In this study, 304 SS welds were treated by UNSM. The residual stress statuses and the microstructures in the near-surface regions before and after UNSM were characterized and compared. In addition, the effects of UNSM on the corrosion resistance of the 304 SS welds in boiling $MgCl_2$ solution were investigated.

CHANG YE is with the Department of Mechanical Engineering, University of Akron, Akron OH 44325-3903. Contact e-mail: cye@uakron.edu ABHISHEK TELANG, AMRINDER GILL, XINGSHUO WEN, SEETHA R. MANNAVA, and VIJAY K. VASUDEVAN are with the Department of Mechanical and Materials Engineering, University of Cincinnati, Cincinnati OH 45221-0072. DONG QIAN is with the Department of Mechanical Engineering, University of Texas at Dallas, Richardson, TX 75080-3021.

Manuscript submitted May 25, 2017.

Article published online January 2, 2018

II. EXPERIMENTAL METHODS

A. Materials

304 SS samples were cut by electric discharge machining (EDM) from two plates of different thickness (1.8 and 2.8 mm). The nominal composition of the material is 0.08 wt pct C, 1.00 wt pct Si, 2.00 wt pct Mn, 0.045 wt pct P, 0.03 wt pct S, 18.0 to 20.0 wt pct Cr, 8.0 to 10.5 wt pct Ni, and balance Fe. SS 304 plates were welded with a single pass butt joint by using gas tungsten arc welding (GTAW) by a commercial sheet metal welding company. SS 308L was used as the filler material. The width of the welds is 10 mm.

B. UNSM Treatment

In the UNSM process (Figure 1(a)), a tungsten carbide ball attached to an ultrasonic unit strikes the metal surfaces at high frequency. The vibration amplitude typically ranges from 8 to 40 μm . At the same time, a static load (typically 10 to 50 N) is applied to the ball against the metal surface. The tungsten carbide ball scans over metal surfaces in a predefined pattern (Figure 1(b)) to make sure the whole surface is uniformly processed. The parameters in a UNSM process include: the static load, the amplitude of the ultrasonic strike, the scan speed, the intervals between neighboring scans (Figure 1(b)), and the ultrasonic peening frequency. UNSM treatment of the welds was carried out after the welds were completely cooled down. In this study, the following parameters were used: the static load was 20 N, the ball diameter was 2.38 mm, the ultrasonic vibration amplitude was 8 μm , the frequency was 20 kHz, the interval was 70 μm and the scanning speed was 3000 mm/min. These parameters were selected based on a previous study.^[14]

C. Characterization

A number of analytical techniques were used to characterize the material's microstructure and properties after UNSM processing as below.

1. Microhardness

The microhardness values of the samples before and after UNSM were measured using a CSM Micro-Nano indentation system with a Berkovich indenter with a maximal load of 500 mN and 10 seconds holding time. Measurements were performed on cross sections of the samples that had been mounted and polished carefully to avoid any damage. An average of five measurements was used for each reported data point.

2. Microstructure observation

Metallographically prepared polished samples were etched using 25 mL HCl + 20 mL CH₃OH + 15 mL HNO₃ solution before microstructure observation. Optical observation was carried out using a Keyence VX-600 digital optical microscope. Electron back scattered diffraction (EBSD) was performed in a FEI XL-30

scanning electron microscope (SEM) using a TSL electron back scatter diffraction/orientation imaging (OIM) system with a high speed Hikari camera.

3. In-depth residual stresses

These residual stresses were measured using conventional X-ray diffraction technique ($\sin^2\Psi$ technique) with layer removal. Proto LXR, a single-axis goniometer, using Ω geometry was used. The alignment of instrument was checked using a standard sample in accordance with ASTM E915-96 ("Verifying the Alignment of X-ray Diffraction Instrumentation for Residual Stress Measurement"). Experimental conditions used were Mn K α radiation, 12 deg Ψ tilts, 3 deg Ψ oscillation to get better statistics, and 1 mm diameter round aperture. The X-ray elastic constant $S_2/2$ used was $7.18 \times 10^{-6} \text{ MPa}^{-1}$ for the austenite phase. Layer removal was done using electropolishing on an area of 10 mm \times 10 mm, using a solution of H₂SO₄ and Methanol (12.5: 87.5 pct by volume). The electropolishing was carried out in an Electro4 Met system from Buehler with a voltage of 24 V. The data were corrected for stress gradients and layer removal in accordance with the SAEJ784a.

4. TEM

For TEM observation of the treated surface, a thin slice ($\sim 250 \mu\text{m}$) was sectioned parallel to the treated surface. This slice was then thinned from the rear to a thickness of $\sim 100 \mu\text{m}$. From this thinned slice, 3 mm disc was obtained using an abrasive slurry disc cutter. The surface of thin slice was covered with a tape to avoid any damage from abrasives. The disc so obtained was dimpled to a thickness of $\sim 15 \mu\text{m}$ and then ion milled at a low angle (12 deg) to electron transparency. TEM observations of the thin foils were carried out using a Philips/FEI CM20 operated at 200 kV.

D. Corrosion Tests

Samples with dimensions of 50 mm by 10 mm were sectioned from the weld plate using wire EDM. Samples were then exposed to boiling MgCl₂ solution (concentration 42 wt pct, temperature 155 °C) for 120 hours or longer. Three samples were UNSM treated and then tested in the same environment to investigate the effect of UNSM on the corrosion behavior. Visual inspection was done every 12 hours to determine the time of failure. After 144 hours or failure (visual inspection with optical microscope), samples were characterized using SEM and EBSD.

III. RESULTS AND DISCUSSION

In this section, we present the effects of UNSM on the microstructure, residual stresses, and corrosion behavior. Further, we discuss these results in the context of use of mechanical surface treatments to mitigate corrosion in SS and its weldments.

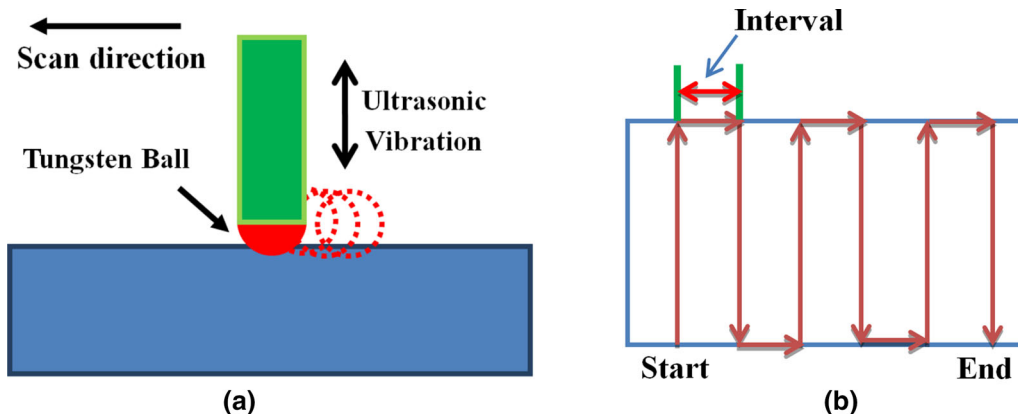


Fig. 1—(a) Schematic setup of the UNSM experiment, (b) scanning pattern of the UNSM process, (the intervals were exaggerated for illustration purpose).

A. Microstructure Evolutions Across the Welding Zone Before and After UNSM

Figure 2 compares the microstructures of the SS 304 welds before and after UNSM. Figures 2(a) and (b) show the microstructure of the welds before UNSM. A transition area between the weld zone and the base metal can be clearly observed in Figure 2(a). In the base material before processing, there was no deformation twins. The weld toe was marked by a white arrow. Figure 2(b) shows the microstructure of the weld, which is typical of austenitic stainless steel welds. Figures 2(c) and (d) show the microstructure across the weld zone after UNSM. In the base material after UNSM, deformation twins can be clearly observed, as pointed by the white arrows in Figure 2(e). In the weld zone, the deformation band morphology is not as clear as in the base material because of the heterogeneous microstructure of the weld. Figure 3 shows the inverse pole figure map of the weld zone and base metal. In both the weld zone and the base metals, random orientation can be observed. Relatively finer grains can be observed in the base metal compared with that in the weld zone.

Figure 4 shows the microstructure observed by TEM in the base material after UNSM. Nanoscale grains can be observed. SAD pattern recorded from the near-surface regions contains reflections forming multiple rings from different crystallographic planes and indicating the polycrystalline nature of the ultrafine/nanoscale grains. According to the optical images in Figure 2(a), the initial grain size is around $30\ \mu\text{m}$. It can be concluded that significant grain refinement in the near-surface regions has been achieved through UNSM, which is consistent with a previous study.^[14] The detailed grain refinement mechanism in stainless steel subjected to plastic deformation has been discussed by Lu and co-workers.^[22] It was suggested that deformation twins play an important role in the grain refinement mechanism. Due to the low stacking fault energy of SS 304, deformation twinning is a preferred deformation mode. In a previous study, highly dense deformation twins were observed in the subsurface of SS 304 after UNSM treatment.^[14] These deformation twins subdivide the

original large grains into submicron blocks, which gradually became subgrain boundaries. Eventually, the subgrain boundaries transformed into nanograins.^[22] It should be noted that only the very top surface has nanocrystalline grains according to a previous study. In addition, how the nanoscale grains affect the corrosion behavior is still controversial in the literature. Further study is needed to investigate the effect of the nanocrystalline surface layer generated by UNSM on the corrosion behavior of SS welds.

B. Residual Stresses

The residual stresses before and after UNSM were analyzed using the $\sin^2\psi$ method.^[23] Figure 5(a) shows the surface residual stresses across the welding zone before and after UNSM. Tensile stresses exist across the welding zone and were generated during the welding process. It can be clearly observed that the tensile residual stresses ranging from 100 to 500 MPa present before UNSM were changed to compressive residual stresses of a high magnitude (-700 to -1300 MPa). Also, it should be noted that the residual stresses before and after UNSM assume a very similar pattern, *i.e.*, the regions that have high tensile stresses before UNSM also have low compressive stresses after UNSM. The highest magnitude of compressive residual stress in the sample after UNSM exists at around 20 mm away from the center of the welding zone. This is because the tensile residual stresses at the same distance were the lowest in the as-welded condition, prior to UNSM.

Due to the symmetry of the residual stress field across the welding zone (Figure 5(a)), the in-depth residual stresses were measured only on one side. A three-dimensional (3D) representation of the in-depth residual stress across the welding zone is shown in Figure 5(b). As we can clearly observe, the magnitude of the compressive residual stress across the welding zone decreases gradually as it goes deeper into the materials. It should be noted that at even $250\ \mu\text{m}$ below the surface, the residual stress is compressive at around -200 to -300 MPa. The existence of compressive residual stress can potentially improve the SCC

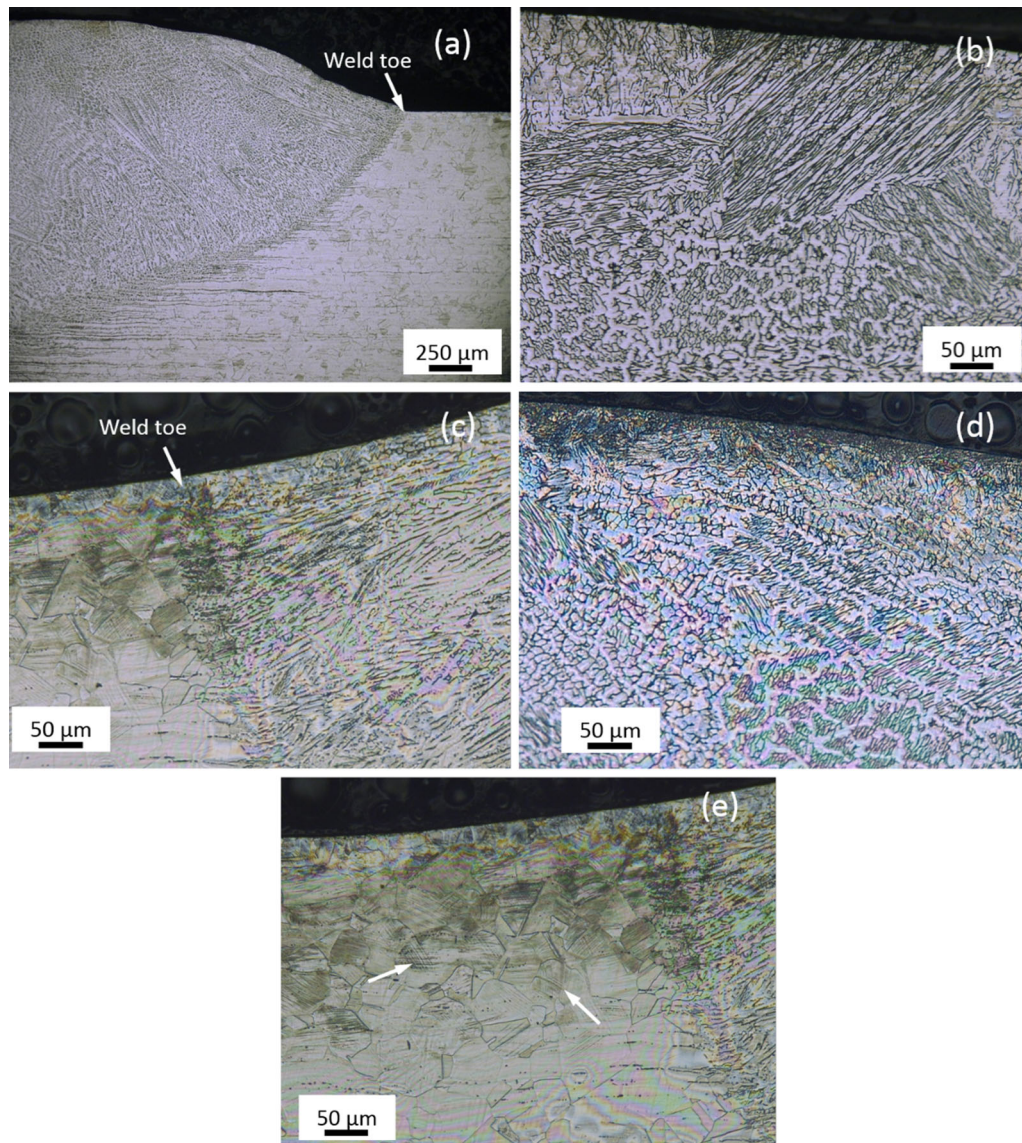


Fig. 2—Optical micrographs showing microstructure across the weld zone before (*a* and *b*) and after (*c*, *d* and *e*) UNSM.

resistance of the material, as has been demonstrated in earlier studies.^[1,7,24,25]

The generation of residual stress consists of two steps: step 1 where the rapid expansion creates sudden compression of the peened area and dilation of the surface layer, and step 2 where the surrounding material reacts to the deformed area, generating a compressive stress field. Various surface severe plastic deformation (SSPD) techniques, including LSP,^[26] SP,^[2] UNSM,^[14] surface mechanical attrition treatment (SMAT), bur-
nishing,^[9] and rolling, have been reported to induce beneficial compressive residual stresses in metals.

C. Hardness Values Across the Welding Zone Before and After UNSM

Figure 6 compares the through-the-depth hardness values in the weld before and after UNSM. The surface hardness increases from around 210 to 400 HV. The

hardness decreases gradually with depth into the welding zone, and gets close to the as-welded sample at around 400 μm below surface.

D. Corrosion Tests

Corrosion tests were performed to evaluate the effects of UNSM on the corrosion resistance without the application of any external stresses. Figure 7 compares the optical micrographs of the as-welded (*a* and *b*) and UNSM-treated (*c* and *d*) samples after testing in boiling MgCl_2 solution. In the as-welded sample, surface morphology becomes very rough due to the formation of the corrosion product. In the UNSM-treated sample, however, surface is still intact without any sign of corrosion. In the as-welded sample, cracks were observed on the sample surface after 72 hours, and the tests were then terminated. Similar tests were also performed on SS 304 weld samples after UNSM

treatment. No cracks were observed in these UNSM-processed samples even after 120 hours of testing in boiling $MgCl_2$ solution. Ghosh and Kain also observed transgranular cracking in as-machined SS304

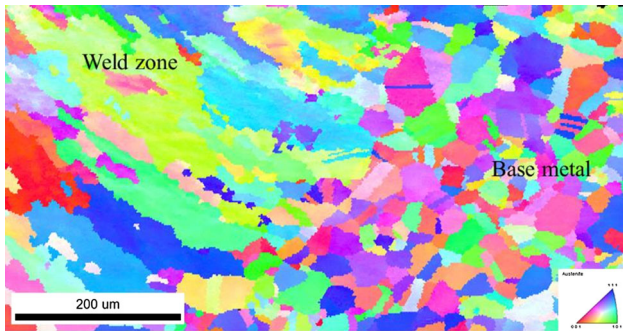


Fig. 3—Inverse pole figure map showing the weld zone and base metal before UNSM treatment.

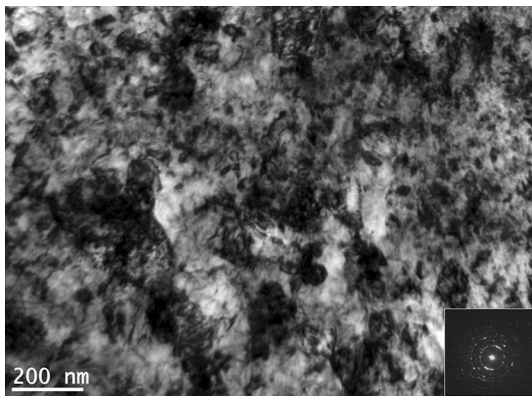


Fig. 4—TEM brightfield image showing the microstructure on the top surface of the base material after UNSM; inset SAD pattern.

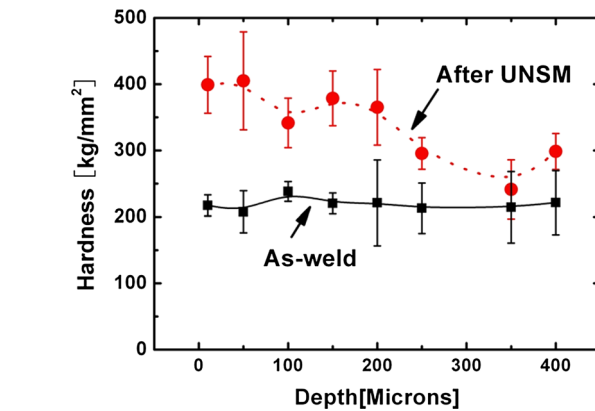
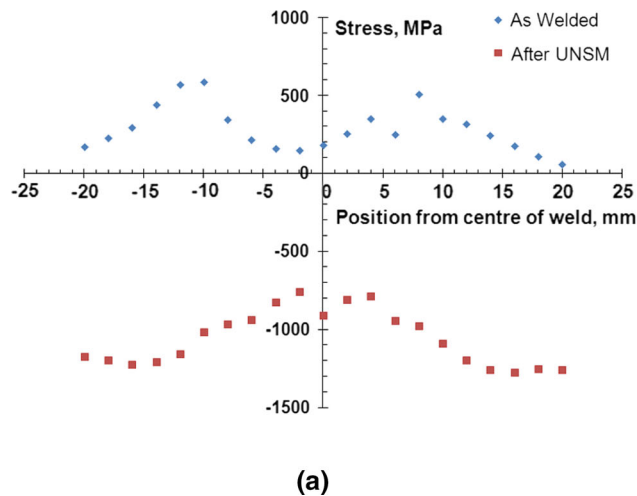


Fig. 6—In-depth microhardness values of the welding zone before and after UNSM, the surface corresponds to the weld center.

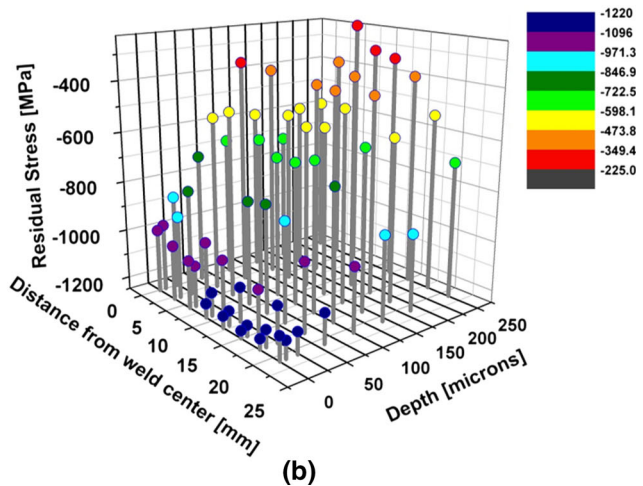


Fig. 5—(a) Surface residual stresses across the welding zone before and after UNSM; (b) 3D residual stress distribution in the welding zone after UNSM.

without any externally applied stress in 48 hours.^[27] They attributed the SCC to the machining-induced residual stresses as the annealed sample did not crack. Ghosh et al. investigated the role of tube manufacturing-induced tensile residual stresses on SCC of SS304 tubes.^[28] Circumferential transgranular cracks were observed in the tubes after 16 hours in boiling $MgCl_2$ solution (155 ± 1 °C) due to tensile residual stresses in the longitudinal direction without any externally applied stresses. Since tensile residual stresses induced by fabrication, machining, and other manufacturing processes have been shown to induce SCC in austenitic stainless steels, mitigation methods involve modifying the nature of residual stresses from tensile to compressive. Obata and Sudo reported the effectiveness of shot peening induced compressive residual stresses on reducing the susceptibility of SCC in $MgCl_2$ environment after shot peening in SS304 welds.^[29] Figure 8 shows an SEM image of the crack and the corresponding (inverse

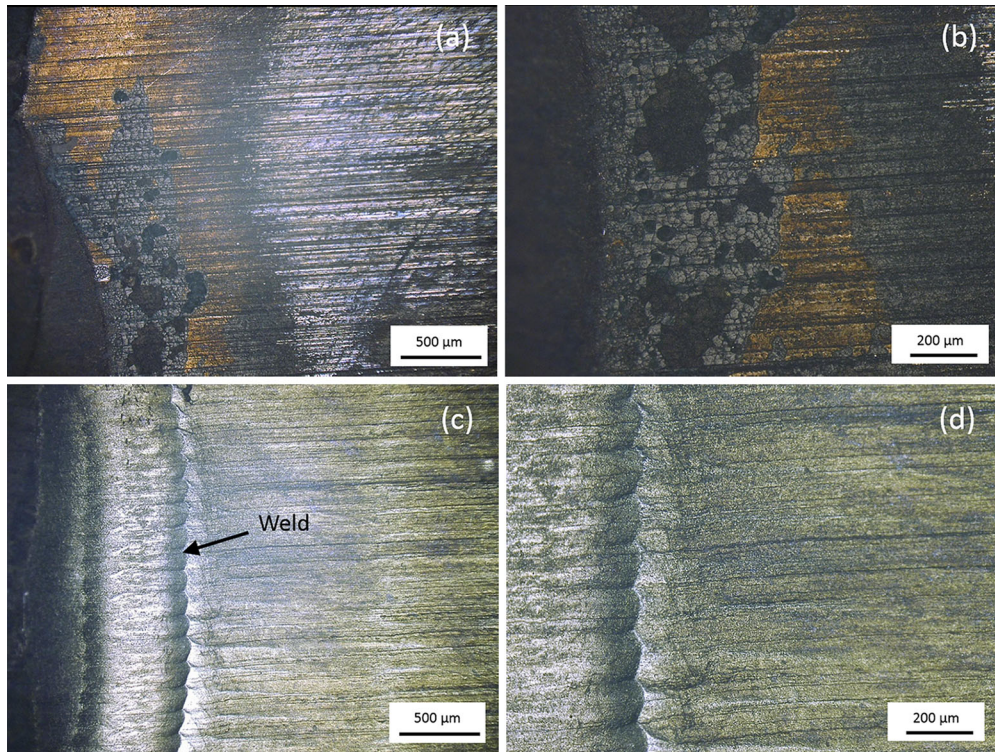


Fig. 7—Optical micrographs of the as-welded (*a* and *b*) and UNSM-treated (*c* and *d*) samples after testing in boiling $MgCl_2$ solution.

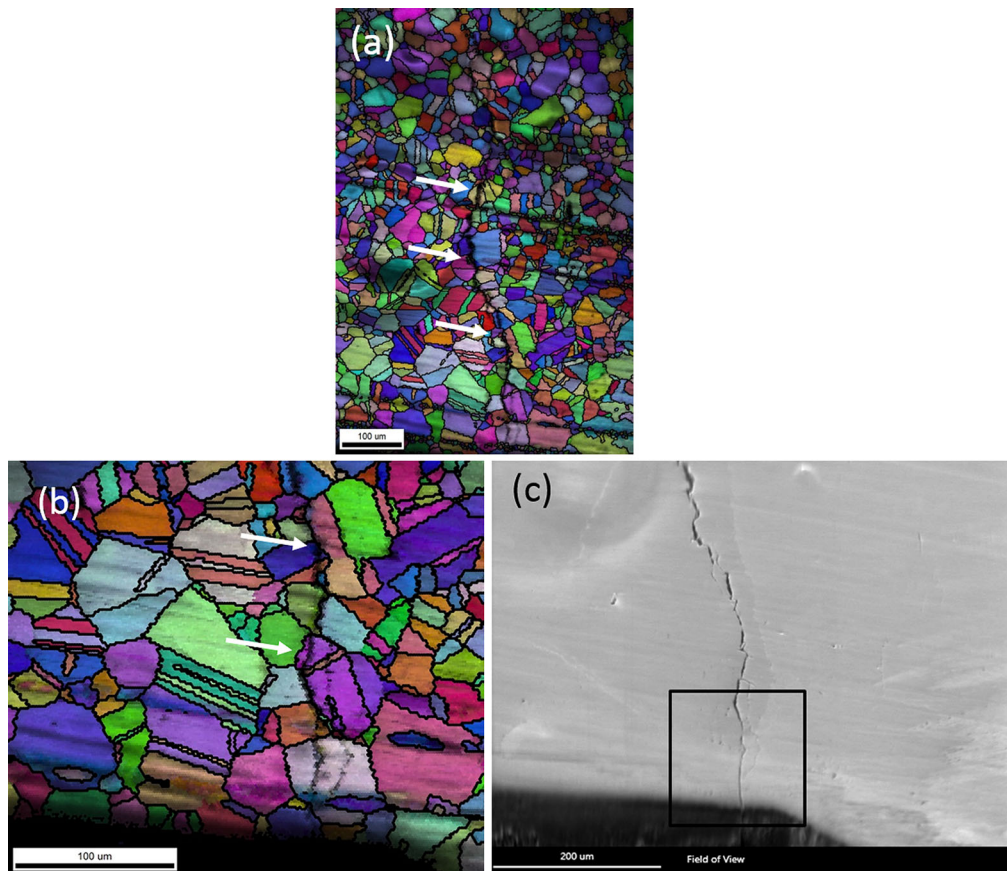


Fig. 8—IPF maps (*a* and *b*) and the corresponding SEM image (*c*) of the as-welded SS 304 sample after corrosion test, grain boundaries are colored black, white arrows showing the transgranular nature of the cracks.

pole figure) IPF maps in the as-welded sample after testing in boiling MgCl_2 solution for 72 hours. From the IPF map, we can clearly observe the transgranular nature of the cracks in the as-welded SS 304 sample. Cracks were observed to have initiated from the surface close to the weld toe, where the residual stresses were tensile, and propagate through the sample thickness in 72 hours. This indicates that the welds were susceptible to chloride corrosion. In the UNSM-treated samples, residual stresses were also measured after corrosion tests to confirm their stability after prolonged exposure to relatively high temperatures. Compressive residual stresses were on the order of -800 to -1200 MPa on the surface of UNSM-treated samples even after 144 hours of exposure to boiling MgCl_2 solution. In contrast, surface residual stresses were on the order of 150 to 450 MPa for the as-welded samples. This explains the improved corrosion resistance after UNSM treatment compared with the as-welded condition.

IV. CONCLUSIONS

UNSM processing of SS 304 welds was carried out in this study. It was demonstrated that UNSM can effectively change the tensile residual stresses into a high magnitude of compressive residual stresses in the weld, heat-affected zone, and base metal regions. In addition, nanocrystallization was observed in the surface region processed by UNSM, together with a large increase in hardness in the near-surface region and up to a depth of $350\ \mu\text{m}$. Corrosion tests in boiling MgCl_2 solution demonstrate that UNSM processing significantly improved the corrosion resistance of the SS 304 welds. Future SCC tests are needed to investigate how UNSM and the associated near-surface microstructures and residual stresses affect the SCC resistance of the welds.

ACKNOWLEDGMENTS

The authors are grateful for financial support to this research by the Nuclear Energy University Program (NEUP) of the US Department of Energy Contract #102835 issued under Prime Contract DE-A-C07-05ID14517 to Battelle Energy Alliance, LLC. The authors also would like to thank the National Science Foundation (Grant # DMR-0706161, CMMI-1335204, 1334538) for financial support to this research. The authors gratefully acknowledge the contribution of the State of Ohio, Department of Development and Third Frontier Commission, which provided funding in support of project: "Ohio Center for Laser Shock Processing for Advanced Materials and Devices," and the permission to avail the experimental and computational equipment facility in the Center to carry out this work. Any opinions, findings, conclusions, or recommendations expressed in these documents are those of the author(s) and do not necessarily reflect the

views of the DOE, NSF, State of Ohio, the Department of Development.

REFERENCES

1. M. Mochizuki: *Nucl. Eng. Des.*, 2007, vol. 237, pp. 107–23.
2. U. Zupanc and J. Grum: *J. Mater. Process. Technol.*, 2010, vol. 210, pp. 1197–1202.
3. P. Peyre, C. Braham, J. Ledion, L. Berthe, and R. Fabbro: *J. Mater. Eng. P*, 2000, vol. 9, pp. 656–62.
4. J.Z. Lu, K.Y. Luo, D.K. Yang, X.N. Cheng, J.L. Hu, F.Z. Dai, H. Qi, L. Zhang, J.S. Zhong, Q.W. Wang, and Y.K. Zhang: *Corros. Sci.*, 2012, vol. 60, pp. 145–52.
5. C. Ye, S. Suslov, B.J. Kim, E.A. Stach, and G.J. Cheng: *Acta Mater.*, 2011, vol. 59, pp. 1014–25.
6. C. Ye, Y. Liao, S. Suslov, D. Lin, and G.J. Cheng: *Mater. Sci. Eng. A*, 2014, vol. 609, pp. 195–203.
7. Y. Sano, M. Obata, T. Kubo, N. Mukai, M. Yoda, K. Masaki, and Y. Ochi: *Mater. Sci. Eng. A*, 2006, vol. 417, pp. 334–40.
8. P. Peyre, X. Scherpereel, L. Berthe, C. Carboni, R. Fabbro, G. Beranger, and C. Lemaitre: *Mater. Sci. Eng. A*, 2000, vol. 280, pp. 294–302.
9. P.S. Prevey and J.T. Cammett: *Int. J. Fatigue*, 2004, vol. 26, pp. 975–82.
10. A. Cherif, Y. Pyoun, and B. Scholtes: *J. Mater. Eng. Perform.*, 2009, vol. 19, pp. 282–86.
11. A. Amanov, Y.S. Pyoun, and S. Sasaki: *Tribol. Int.*, 2014, vol. 72, pp. 187–97.
12. A. Gill, A. Telang, S.R. Mannava, D. Qian, Y.-S. Pyoun, H. Soyama, and V.K. Vasudevan: *Mater. Sci. Eng. A*, 2013.
13. X.J. Cao, Y.S. Pyoun, and R. Murakami: *Appl. Surf. Sci.*, 2010, vol. 256, pp. 6297–6303.
14. C. Ye, A. Telang, A.S. Gill, S. Suslov, Y. Idell, K. Zwiack, J.M.K. Wiezorek, Z. Zhou, D. Qian, S.R. Mannava, and V.K. Vasudevan: *Mater. Sci. Eng. A*, 2014, vol. 613, pp. 274–88.
15. C. Ye, X. Zhou, A. Telang, H. Gao, Z. Ren, H. Qin, S. Suslov, A.S. Gill, S.R. Mannava, D. Qian, G.L. Doll, A. Martini, N. Sahai, and V.K. Vasudevan: *J. Mech. Behav. Biomed. Mater.*, 2016, vol. 53, pp. 455–62.
16. H. Zhang, R. Chiang, H. Qin, Z. Ren, X. Hou, D. Lin, G.L. Doll, V.K. Vasudevan, Y. Dong, and C. Ye: *Int. J. Fatigue*, 2017, vol. 103, pp. 136–46.
17. C. Ma, H. Qin, Z. Ren, S.C. O'Keefe, J. Stevick, G.L. Doll, Y. Dong, B.B. Winiarski, C. Ye, S.C. O'Keefe, J. Stevick, G.L. Doll, Y. Dong, B.B. Winiarski, C. Ye, S.C. O'Keefe, J. Stevick, G.L. Doll, Y. Dong, B.B. Winiarski, and C. Ye: *J. Alloys Compd.*, 2017, vol. 718, pp. 246–53.
18. A. Amanov, O.V. Penkov, Y.-S. S. Pyoun, and D.-E.E. Kim: *Tribol. Int.*, 2012, vol. 54, pp. 106–13.
19. X. Hou, H. Qin, H. Gao, S. Mankoci, R. Zhang, X. Zhou, Z. Ren, G.L. Doll, A. Martini, N. Sahai, Y. Dong, and C. Ye: *Mater. Sci. Eng. C*, 2017, vol. 78, pp. 1061–71.
20. Y.-S. Kim, W.-C. Kim, and J.-G. Kim: *CORROSION*, 2017.
21. S. Li, Z. Ren, Y. Dong, C. Ye, G. Cheng, and H. Cong: *J. Electrochem. Soc.*, 2017, vol. 164, pp. C682–89.
22. J.Z. Lu, K.Y. Luo, Y.K. Zhang, G.F. Sun, Y.Y. Gu, J.Z. Zhou, X.D. Ren, X.C. Zhang, L.F. Zhang, K.M. Chen, C.Y. Cui, Y.F. Jiang, A.X. Feng, and L. Zhang: *Acta Mater.*, 2010, vol. 58, pp. 5354–62.
23. B.D. Cullity: *Elements of X-Ray Diffraction*, 2nd ed., Addison-Wesley Publishing Company Inc, Reading, MA, 1978.
24. A. Telang, A.S. Gill, S. Teyseyre, S.R. Mannava, D. Qian, and V.K. Vasudevan: *Corros. Sci.*, 2015, vol. 90, pp. 434–44.
25. A. Telang, A.S. Gill, D. Tammana, X. Wen, M. Kumar, S. Teyseyre, S.R. Mannava, D. Qian, and V.K. Vasudevan: *Mater. Sci. Eng. A*, 2015, vol. 648, pp. 280–88.
26. J. Zhao, Y. Dong, and C. Ye: *Int. J. Fatigue*, 2017, vol. 100, pp. 407–17.
27. S. Ghosh and V. Kain: *J. Nucl. Mater.*, 2010, vol. 403, pp. 62–67.
28. S. Ghosh, V.P.S. Rana, V. Kain, V. Mittal, and S.K. Baveja: *Mater. Des.*, 2011, vol. 32, pp. 3823–31.
29. M. Obata and A. Sudo: in *Proc. ICSP-5 Conf. Oxford, UK*, 1993, pp. 257–64.